The Aeronautical Journal (2022), **126**, pp. 475–499
doi:10.1017/aer.2021.79

REGULAR PAPER

Simulink-based simulation platform design and faults impact analysis of attitude control systems

H. Song[1], S.L. Hu[2,3,*] and W.Z. Chen[1]

[1]School of Automation and Information Engineering, Xi'an University of Technology, Xi'an, 710048, China, [2]School of Automation, Guangdong University of Petrochemical Technology, Maoming, 528000, China and [3]School of Artificial Intelligence, Henan University, Kaifeng, 475001, China
*Corresponding: hfkth@126.com

Received: 1 February 2021; **Revised:** 31 July 2021; **Accepted:** 5 August 2021

Keywords: attitude control systems; reaction flywheels; attitude sensors; system simulation

Abstract

The satellite attitude control system (SACS) is a complicated system. In order to reflect the relationship among different components in SACS and analyse the impact of component faults on system performance, a complete simulation platform of the SACS based on Simulink is built in this paper. With the embedding of the specific reaction flywheel, gyroscope and earth sensor model, and the design of the controller based on the quaternion feedback, the simulation platform can not only simulate the real SACS at the component level, but it can also realise the injection of component faults for analysing the system performance. Simulations are conducted to verify the performance of the simulation platform. Simulation results show that this simulation platform has the ability to accurately reflect the control performance of the SACS, and the output accuracy of the component model is high. The research results reveal that this simulation platform can provide model support for verifying the algorithm of fault diagnosis, prediction and tolerant control of the SACS. This simulation platform is easy to use and can be expanded and improved.

1.0 Introduction

As a main subsystem of the satellite, the attitude control system primarily undertakes two important tasks: attitude stabilisation and attitude control, and it mainly include an attitude measurement system and actuator control system [1]. The SACS is a complicated and sophisticated system that increases the difficulty of design. Since the components of the SACS will fail, it is essential to use digital simulation methods to verify the stability and reliability of the system by establishing a more accurate mathematical simulation model for the SACS. According to the type of faults in the SACS, the method of artificial fault injection is used to simulate and analyse the state change of the SACS, and corresponding precautions are given to ensure the safety of satellites in orbit for a long time.

Based on the computer-aided analysis, the mathematical modelling and simulation analysis of the partial structure of the SACS had been completed, such as the orbital environment, attitude dynamics and kinematics, measurement and control algorithms, and some physical objects were accessed to simulate the control effect of the satellite attitude [2]. Yu and Liang realised the simulation design of the attitude control system of the satellite jet and completed the mathematical modelling and simulation analysis of the corresponding attitude dynamics and controller in the Simulink library [3]. Based on the motion module of six degree of freedom (6-Dof) in the Simulink library of Matlab software, Bai and Bei realised the simulation of the SACS in the rate damping stage and the three-axis stabilisation stage, and completed the model of the attitude dynamics, thrusters and actuators [4]. The function modules of the Simulink library were used to build the simulation system for simulating the space environment

© The Author(s), 2021. Published by Cambridge University Press on behalf of Royal Aeronautical Society.

https://doi.org/10.1017/aer.2021.79 Published online by Cambridge University Press

and the attitude dynamics model, the physical platform including the controller and measurement components has been established, finally, the semi-physical simulation of the SACS was achieved [5,6]. In addition, the Satellite Tool Kit (STK) software was also used for modelling and simulation of the SACS [7]. Based on the STK and Laboratory Virtual Instrument Engineering Workbench (LabVIEW), He et al. completed the design of a visual simulation platform for satellite orbit prediction and achieved the three-dimensional display of the spacecraft [8]. The STK, LabVIEW, three-axis Helmholtz coil (HC3), satellite (CubeSat) and integrator were connected to form a simulation system of the SACS. Among them, the STK was mainly used for generating the analog value of the in-orbit magnetic field based on the attitude quaternion [9]. Ure and Kaya introduced how software and hardware of the SACS can be connected to the simulation system [10]. Among them, STK was used to generate space position and magnetic field value of the satellite and provided the simulation input of the environment.

In summary, the above-mentioned simulation platform of the SACS based on Simulink lacks specific actuator and attitude sensor models. These simulation platforms are not complete and cannot fully reflect the connection relationship and working status of the components, so they are not suitable for components simulation and faults injection. The STK is not suitable for attitude simulation. The STK is difficult to provide attitude simulation data, and it is also difficult to build a complete simulation model of the SACS that includes specific actuators and attitude measurement components, as well as specific attitude determination and control algorithms. Therefore, in order to overcome the shortcomings and limitations of existing software to realise the simulation of the SACS, we build a complete simulation platform based on Simulink that can simulate the SACS at the component level and complete the simulation analysis of the effect of component faults on the system performance.

The structure of this paper is as follows. In section II, the simulation models are established, such as actuator model, attitude sensor model, controller model, attitude dynamics and kinematic model and attitude determination model, and form a complete simulation platform of the SACS. In section III, the numerical simulation is executed to verify the performance of the simulation platform and analyse the influence of component faults on the performance of the SACS. Finally, conclusions are drawing in section 4.

2.0 Design of simulation platform for sacs

Taking the three-axis-stabilised SACS as an example, the simulation platform was design and its performance was analysed. The three-axis-stabilised satellite means that the satellite is stable in the three directions of X, Y and Z relative to the orbital coordinate system; in other words, the satellite maintains a certain attitude relationship with the earth. However, in order to ensure the stability of the satellite, some attitude control equipment (thrusters, momentum wheel and so on) had been increased to control the attitude change.

2.1 Design ideology

The simulation structure of the three-axis-stabilised SACS is shown in Fig. 1. According to the measurement information of the attitude sensor, the attitude determination algorithm is used to determine the attitude parameters (attitude angle and angular velocity) of the three-axis-stabilised satellite; the error between the current attitude parameters and the desired attitude parameters is used to trigger the controller to generate a control signal, and this control signal is used to drive the actuator to generate control torque; the control torque is used to update the attitude parameters until the satellite reaches the desired attitude. [11,12]

2.2 Sub-model design of simulation platform

Based on the simulation structure of the SACS, the actuator and attitude sensor are determined. The function modules in the Simulink library are used to establish sub-model; finally, a complete simulation

https://doi.org/10.1017/aer.2021.79 Published online by Cambridge University Press

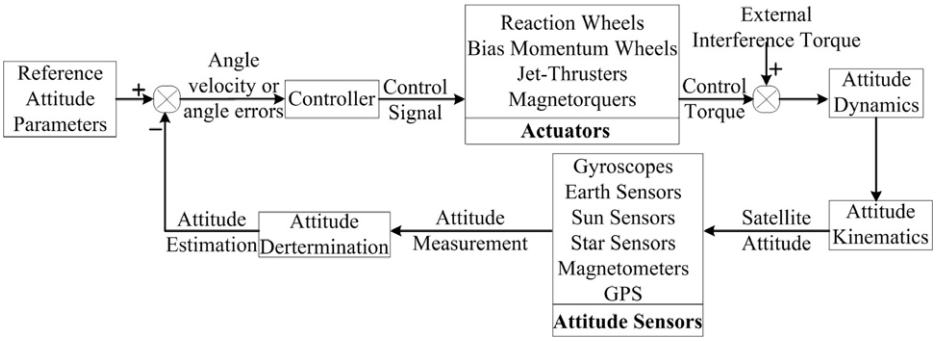


Figure 1. *Simulation structure of three-axis stabilised SACS.*

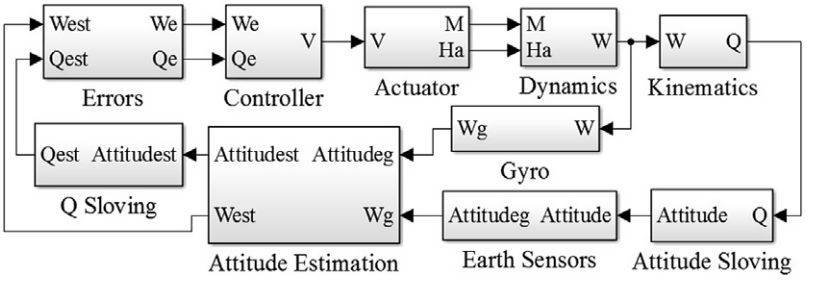


Figure 2. *Simulation platform of the SACS.*

platform of the SACS is shown in Fig. 2. Among them, the gyroscope and earth sensor model are used to output the information of the attitude dynamics and kinematics model, the attitude estimation model can determine the current attitude, the controller model uses the error information to output a control voltage signal, and the actuator model generates control torque to update the attitude parameters of the satellite.

2.2.1 Actuators model

At present, the actuator of the three-axis-stabilised SACS generally uses the angular momentum exchange device, which called as the wheel control system. [12] Considering the torque-type reaction flywheel with three-axis orthogonal fixed installation, an accurate torque balance equation needs to be introduced [13], so as to describe the output torque M_m of the reaction flywheel accurately.

$$M_m = M_c + M_f + M_x + M_a + M_d \tag{1}$$

where M_c is flywheel control torque, M_f is friction torque, M_x is noise torque, M_a is aerodynamic drag torque and M_d is dynamic unbalance torque.

Briefly, the armature inductance is L, the armature resistance is R, the armature current is $i(t)$, the opposing electromotive force is $e(t)$, the control voltage is $u(t)$, and the torque moment coefficient is K_m (N∗m/A). The voltage balance equation of reaction flywheel can be given [13]:

$$\begin{cases} L\dfrac{di\,(t)}{dt} + Ri\,(t) + e\,(t) = u\,(t) \\ M_m = K_m i\,(t) \end{cases} \tag{2}$$

According to the Laplace transformation, a function relationship between the control voltage V and the motor output torque M_m is obtained.

$$M_m = K_m \frac{V}{Ls + R} \tag{3}$$

https://doi.org/10.1017/aer.2021.79 Published online by Cambridge University Press

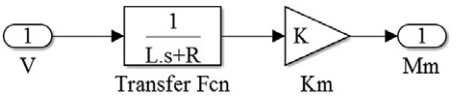


Figure 3. *Simulation module of output torque and control voltage.*

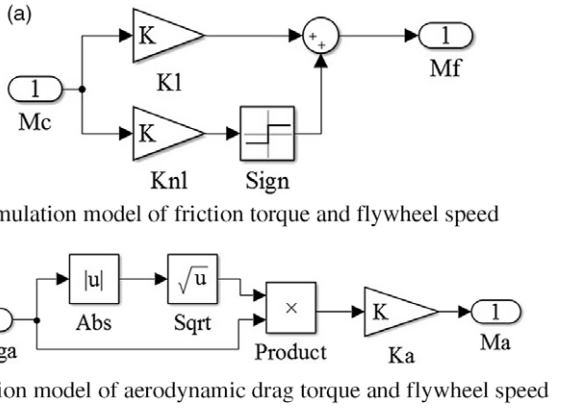


Figure 4. *Simulation model of torque and flywheel.*

Based on equation (3), the simulation module in the Simulink is showed in Fig. 3.

Sign the linear friction coefficient is K_l, the nonlinear friction coefficient is K_{nl}, the noise coefficient is K_x, the zero mean white noise is W, the aerodynamic drag coefficient is K_a and the dynamic unbalance coefficient is K_d. The function relationship between the different torque and the rotational speed Ω in the reaction flywheel [13–15] is shown in equation (4):

$$\begin{cases} M_f = K_l\Omega + K_{nl} sign\ (\Omega) \\ M_x = K_x\ (W/\ |W_{\max}|) \\ M_a = K_a\Omega\sqrt{|\Omega|} \\ M_d = K_d\Omega^2 \sin\ (\Omega t) \end{cases} \tag{4}$$

Based on equation (4), the functional relationship between various torque and flywheel speed can be modeled in the Simulink is showed in Fig. 4.

The rotational speed Ω of reaction flywheel can be integrated by the torque balance equation (14):

$$\Omega = J_c^{-1} \int M_c dt \tag{5}$$

where, J_c is the moment of inertia of reaction flywheel (kg^*m^2).

Based on equation (5), the simulation model in the Simulink is showed in Fig. 5.

Based on the above analysis and the reference [14], the simulation model of reaction flywheel is showed in Fig. 6. Among them, the input 1 is the motor control voltage V, the output 1 is the control torque M_c of reaction flywheel, and the output 2 is the angular momentum H_a of reaction flywheel.

https://doi.org/10.1017/aer.2021.79 Published online by Cambridge University Press

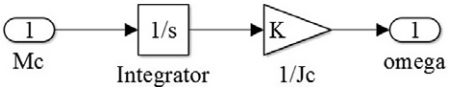


Figure 5. *Simulation model of control torque and flywheel speed.*

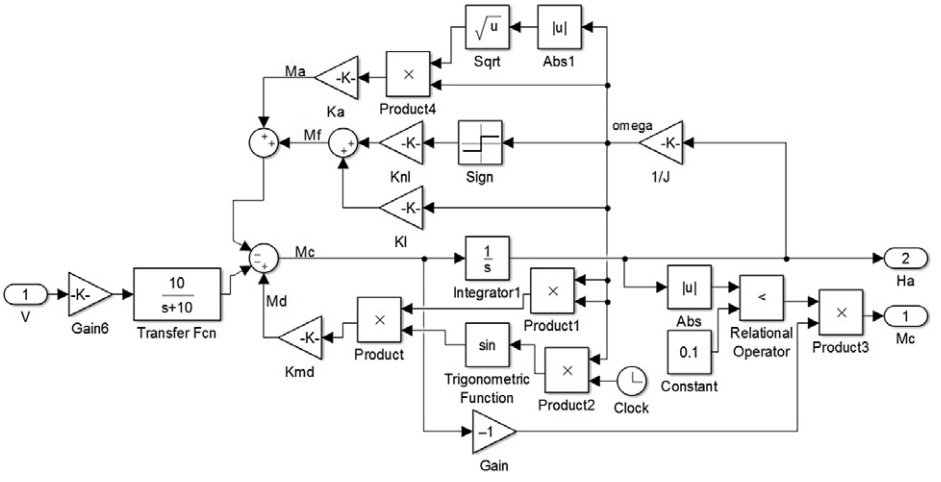


Figure 6. *Simulation model of reaction flywheel [14].*

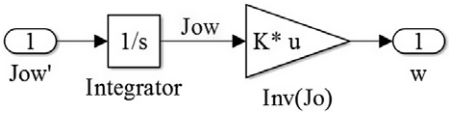


Figure 7. *Simulation model of satellite angular velocity.*

2.2.2 Attitude dynamics model

Attitude dynamics studies the rotational motion of a satellite around its mass center under the action of external and internal torques, which not only studies the overall attitude motion of the satellite, but also studies the relative motion among various parts of the satellite [12]. The attitude dynamics is also related closely to the satellite structure. Regardless of the influence of the flexibility vibration, liquid fuel tank size and installation position on the attitude dynamics of the satellite, a simulation model of the attitude dynamics is established.

The dynamics equation of a satellite with flywheel can be described as follows [12]:

$$J_o\dot{\Omega} + J_c\dot{\omega} + \omega \times (J_o\omega + J_c\Omega) = M \tag{6}$$

where, J_o is the moment of inertia matrix of satellites, ω=$[\omega_x\ \omega_y\ \omega_z]^T$ is the rotational angular velocity of satellites, M is the external torque of satellites.

The control torque M_c of reaction flywheel is $J_c\dot{\Omega}$, so, equation (6) can be rewritten as:

$$J_o\dot{\omega} + \omega \times (J_o\omega + J_c\Omega) = M - M_c \tag{7}$$

We can integrate $J_o\dot{\omega}$ to obtain $J_o\omega$ and then multiply the inverse $inv(J_o)$ of moment of inertia matrix of satellite to obtain rotational angular velocity ω, and its model in the Simulink is showed in Fig. 7.

The cross-multiplication of $H = J_o\omega + J_c\Omega$ and the angular velocity ω can be implemented in the Simulink, the simulation model is showed in Fig. 8.

https://doi.org/10.1017/aer.2021.79 Published online by Cambridge University Press

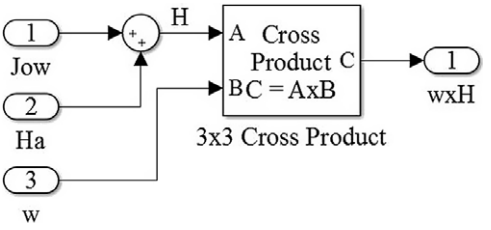


Figure 8. *Simulation model of the cross-multiplication of momentum torque and angular velocity.*

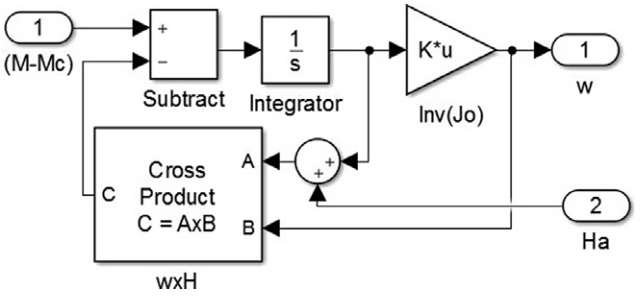


Figure 9. *Simulation model of satellite attitude dynamics with wheel [14].*

Based on the above analysis and the reference [14], the simulation model of attitude dynamics is showed in Fig. 9. Among them, the input 1 is the error (M-M_c) between the external torque M and the control torque M_c, the input 2 is the momentum moment H_a of reaction flywheel, and the output 1 is the rotational angular velocity ω of the satellite.

2.2.3 Attitude kinematics model

When describing the change of the attitude, the method based on the quaternion only needs four parameters, and this method is no singular position; therefore, it is widely used to establish the attitude kinematics of satellites [12].

After the satellite rotates a certain angle around a certain axis, the Euler quaternion is defined as $\boldsymbol{q}=[q_0\ q_1\ q_2\ q_3]^T$.

$$\begin{cases} q_0 = \cos\left(\frac{\Phi}{2}\right) q_1 = e_x \sin\left(\frac{\Phi}{2}\right) \\ q_2 = e_y \sin\left(\frac{\Phi}{2}\right) q_3 = e_z \sin\left(\frac{\Phi}{2}\right) \end{cases} \tag{8}$$

where, Φ is the rotation angle, ($e_x\ e_y\ e_z$) is the unit direction vector of rotation axis.

As ${e_x}^2 + {e_y}^2 + {e_z}^2 = 1$, the quaternion satisfies the orthogonal constraint equation.

$${q_0}^2 + {q_1}^2 + {q_2}^2 + {q_3}^2 = 1 \tag{9}$$

The quaternion $\boldsymbol{q}$ satisfies the above constraint called normalised quaternion.

Let the satellite rotate in the order of Z-X-Y, the kinematics equation of satellite attitude based on quaternion can be described:

$$\begin{bmatrix} \dot{q}_0 \\ \dot{q}_1 \\ \dot{q}_2 \\ \dot{q}_3 \end{bmatrix} = \frac{1}{2} \begin{bmatrix} 0 & -\omega_x & -\omega_y & -\omega_z \\ \omega_x & 0 & \omega_z & -\omega_y \\ \omega_y & -\omega_z & 0 & \omega_x \\ \omega_z & \omega_y & -\omega_1 & 0 \end{bmatrix} \begin{bmatrix} q_0 \\ q_1 \\ q_2 \\ q_3 \end{bmatrix} \tag{10}$$

https://doi.org/10.1017/aer.2021.79 Published online by Cambridge University Press

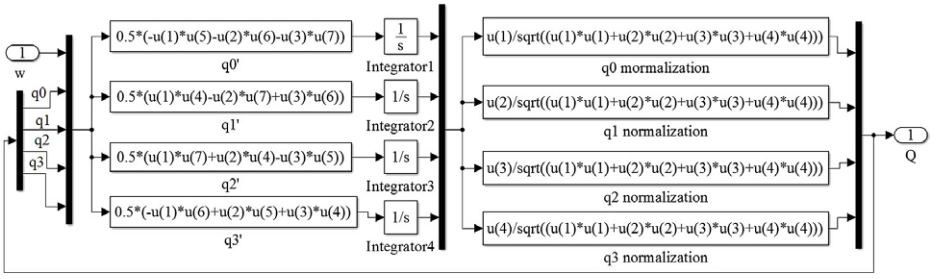


Figure 10. *Simulation model of attitude kinematics based on quaternion.*

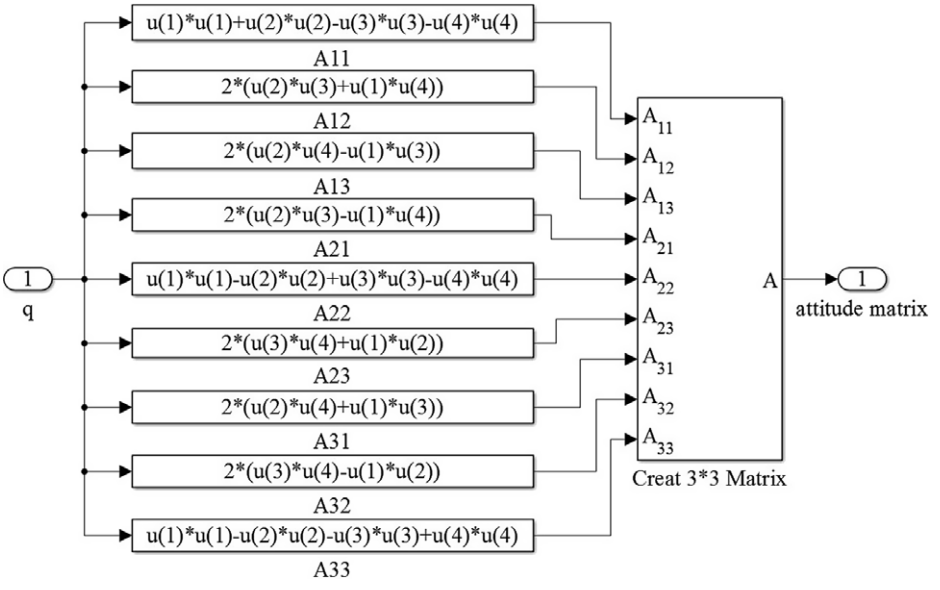


Figure 11. *Simulation model of attitude matrix based on quaternion.*

Taking the attitude angular velocity and quaternion as input, the current attitude quaternion can be obtained through integration and regularisation. According to equations (9), (10) and reference [16], the simulation model of attitude kinematics based on quaternion in the Simulink is showed in Fig. 10.

The attitude matrix can be used to convert the attitude quaternion into the attitude Euler angle. The attitude matrix based on quaternion can be given [12]

$$A = \begin{bmatrix} q_0^2 + q_1^2 - q_2^2 - q_3^2 & 2(q_1q_2 + q_3q_0) & 2(q_1q_3 - q_2q_0) \\ 2(q_1q_2 - q_3q_0) & q_0^2 - q_1^2 + q_2^2 - q_3^2 & 2(q_2q_3 + q_1q_0) \\ 2(q_1q_3 + q_2q_0) & 2(q_2q_3 - q_1q_0) & q_0^2 - q_1^2 - q_2^2 + q_3^2 \end{bmatrix} \tag{11}$$

Based on equation (11) and reference [16], the simulation model of attitude matrix in the Simulink is showed in Fig. 11.

The functional relationship between the attitude matrix and the attitude angle can be given [12]:

$$\begin{bmatrix} \varphi \\ \theta \\ \psi \end{bmatrix} = \begin{bmatrix} arctg_2\left(2(q_0q_1 + q_2q_3), 1 - 2\left(q_1^2 + q_2^2\right)\right) \\ \arcsin\left(2(q_0q_2 - q_3q_1)\right) \\ arctg_2\left(2(q_0q_3 + q_1q_2), 1 - 2\left(q_2^2 + q_3^2\right)\right) \end{bmatrix} \tag{12}$$

Based on equation (12) and reference [16], the simulation model in the Simulink is showed in Fig. 12.

https://doi.org/10.1017/aer.2021.79 Published online by Cambridge University Press

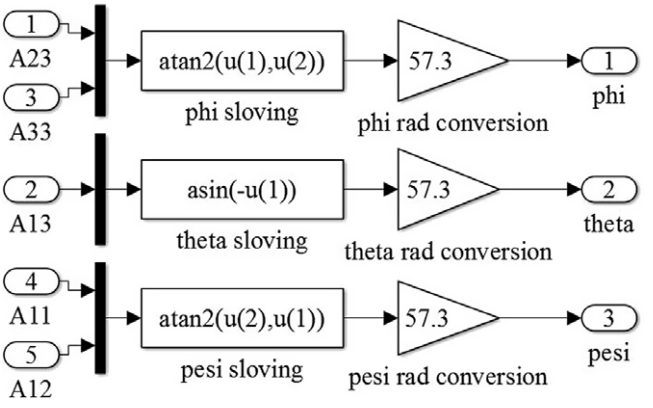


Figure 12. *Simulation model of attitude angle based on quaternion.*

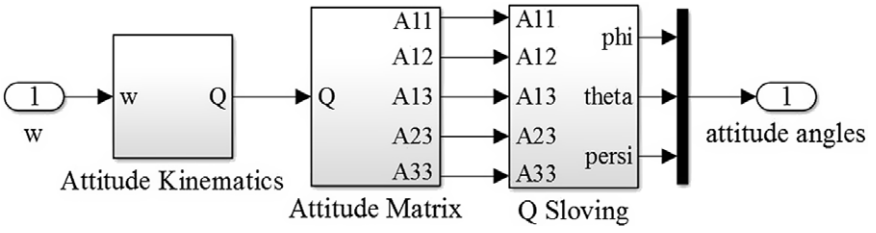


Figure 13. *Simulation model of attitude angle solving based on quaternion.*

Based on the above analysis, we take the attitude angular velocity as the input and establish the simulation model of attitude kinematics based on quaternion, so as to calculate the attitude angle. The simulation model is showed in Fig. 13.

2.2.4 Gyroscopes model

The three-rate integral gyros are used to measure the angular velocity of the satellite, which are parallel to the three axes of the satellite and are installed orthogonally to each other. The measurement model of the gyroscope can be given [17, 18]:

$$\begin{cases} \omega_g = \omega + b + d + n_g \\ \dot{d} = -Dd + n_d \end{cases} \tag{13}$$

where, ω_g is the measured angular velocity of gyros, b is the constant drifting of gyros, n_g is the measured noise of gyros, d is the random drifting of gyros, n_d is the noise of random drifting and D=$diag(1/\tau_x\ 1/\tau_y\ 1/\tau_z)$ is the diagonal matrix formed by the correlation time constant $\tau_i(i = x,y,z)$.

Based on equation (13), the simulation model in the Simulink is showed in Fig. 14. Among them, the input 1 is the angular velocity ω of the satellite, and the output 1 is the measured angular velocity ω_g of the gyros.

2.2.5 Earth sensors model

The earth sensors are used to measure the attitude angles of the satellite. The two earth sensors have been adopted to measure the roll angle φ and pitch angle θ of the satellite. The measured model of earth sensors can be given [19, 20]

$$\begin{cases} \varphi_e = \varphi + \varphi_b + \varphi_n \\ \theta_e = \theta + \theta_b + \theta_n \end{cases} \tag{14}$$

https://doi.org/10.1017/aer.2021.79 Published online by Cambridge University Press

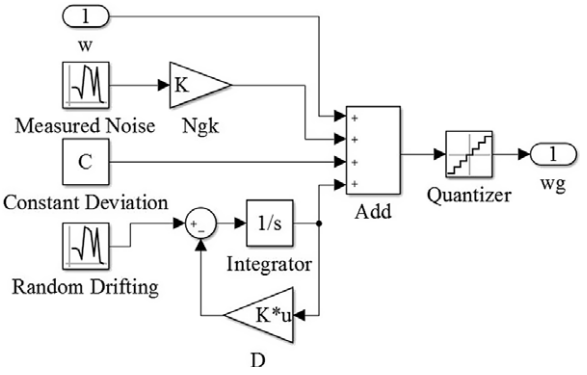


Figure 14. *Simulation model of the gyros [14].*

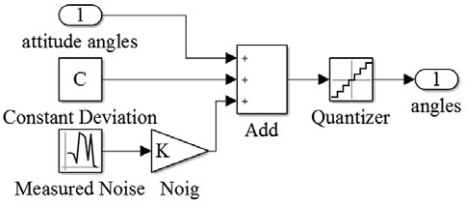


Figure 15. *Simulation model of the earth sensor [14].*

where, φ_e and θ_e is the measured output of earth sensors, φ_b and θ_b is the constant deviation of earth sensors, φ_n and θ_n is the measured noise of earth sensors.

Based on equation (14), the simulation model in the Simulink is showed in Fig. 15. Among them, the input 1 is the φ and θ of the satellite, the output 1 is the measured angle φ_e and θ_e of earth sensors.

2.2.6 Attitude determination model

According to the principle of the attitude determination based on the gyroscope and the earth sensor, and the design method of the state observer in modern control theory [12], the estimation value $(\hat{\varphi}\ \hat{\theta}\ \hat{\psi})$ of the roll, pitch and yaw angle can be obtained:

$$\begin{cases} \dot{\hat{\varphi}} = \omega_o \hat{\psi} + \omega_{gx} + K_\varphi(\varphi_m - \hat{\varphi}) \\ \dot{\hat{\theta}} = \omega_o + \omega_{gy} + K_\theta(\theta_m - \hat{\theta}) \\ \dot{\hat{\psi}} = -\omega_o \hat{\varphi} + \omega_{gz} + K_\psi(\varphi_m - \hat{\varphi}) \end{cases} \tag{15}$$

where, $(\dot{\hat{\varphi}}\ \dot{\hat{\theta}}\ \dot{\hat{\psi}})$ is the estimation value of attitude angular velocity, ω_o is the instantaneous angular velocity of the satellite, $(K_\varphi\ K\theta\ K\psi)$ is the gain coefficient and its value is $0.005\sim0.05(1/s)$.

Based on equation (15), the simulation model of the attitude determination in the Simulink is showed in Fig. 16. Among them, the input 1 is the measured angle φ_e and θ_e of earth sensors, the input 2 is the measured angular velocity ω_g of gyroscopes, the output 1 is the estimation value $(\hat{\varphi}\ \hat{\theta}\ \hat{\psi})$ of attitude angles, the output 2 is the estimation value $(\dot{\hat{\varphi}}\ \dot{\hat{\theta}}\ \dot{\hat{\psi}})$ of attitude angular velocity.

The conversion relationship between the attitude Euler angle and the quaternion is as follows.

$$q = \begin{bmatrix} q_0 \\ q_1 \\ q_2 \\ q_3 \end{bmatrix} = \begin{bmatrix} \cos(\varphi/2)\cos(\theta/2)\cos(\psi/2) + \sin(\varphi/2)\sin(\theta/2)\sin(\psi/2) \\ \sin(\varphi/2)\cos(\theta/2)\cos(\psi/2) - \cos(\varphi/2)\sin(\theta/2)\sin(\psi/2) \\ \cos(\varphi/2)\sin(\theta/2)\cos(\psi/2) + \sin(\varphi/2)\cos(\theta/2)\sin(\psi/2) \\ \cos(\varphi/2)\cos(\theta/2)\sin(\psi/2) - \sin(\varphi/2)\sin(\theta/2)\cos(\psi/2) \end{bmatrix} \tag{16}$$

Based on equation (16), the simulation model in the Simulink is showed in Fig. 17.

https://doi.org/10.1017/aer.2021.79 Published online by Cambridge University Press

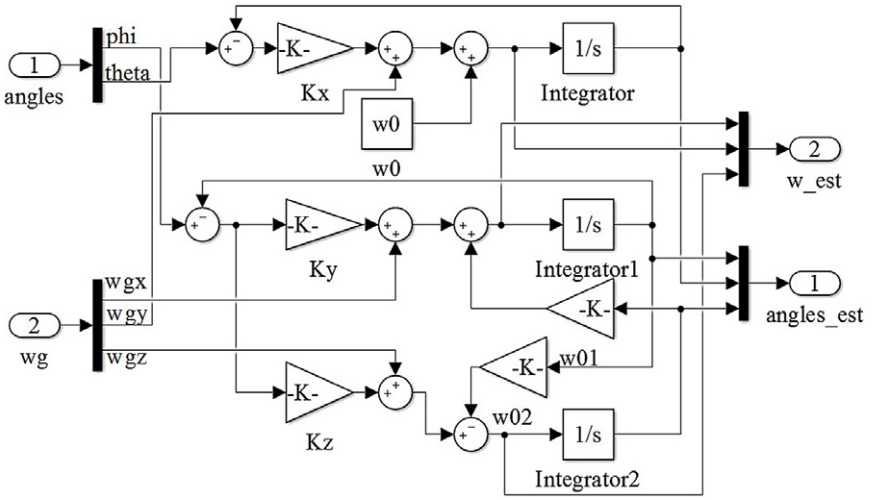


Figure 16. *Simulation model of attitude determination [14]'.*

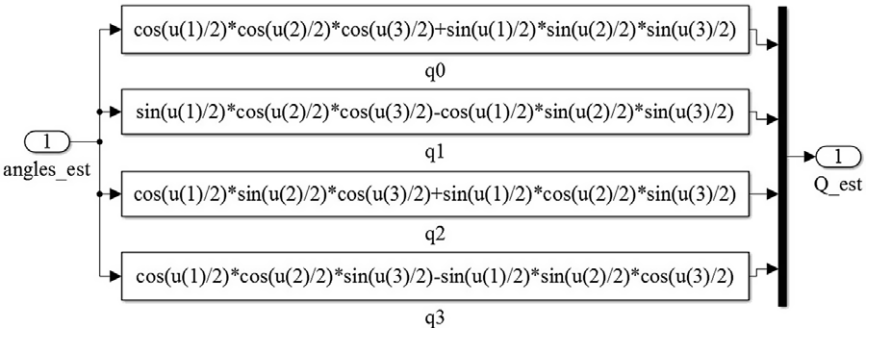


Figure 17. *Simulation model of attitude quaternion solving.*

2.2.7 Controller model

Assuming that the current quaternion is $\boldsymbol{Q}$, the desired attitude quaternion is $\boldsymbol{Q}_d$, the error quaternion $\boldsymbol{Q}_e$ can be expressed as [21]

$$\begin{aligned} Q_e &= Q_d{}^* Q \\ &= \begin{bmatrix} q_{d0}q_0 - q_d{}^T q \\ q_d q_0 + q_{d0} q + q_d \times q \end{bmatrix} \end{aligned} \tag{17}$$

where, $\boldsymbol{Q}_d{*}{=}[q_{d0}\ \text{-}\boldsymbol{q}_d]^T$ and $\boldsymbol{Q}{=}[q_0\ \boldsymbol{q}]^T$.

Based on equation (17), the simulation model in the Simulink is showed in Fig. 18.

In order to quickly capture the dynamic performances of the attitude changes and enable the satellite attitude to quickly stabilise to the desired position, we choose the PD controller [22]. The error quaternion and error angular velocity are used as the control variables, and the control law is designed.

$$u = -K_p q_e - K_d \omega_e \tag{18}$$

where, $\boldsymbol{K}_p$ and $\boldsymbol{K}_d$ are the control coefficients.

https://doi.org/10.1017/aer.2021.79 Published online by Cambridge University Press

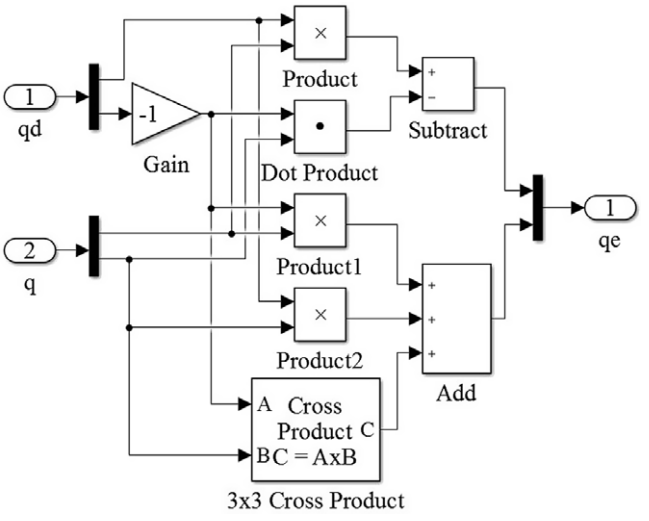


Figure 18. *Simulation model of error quaternion.*

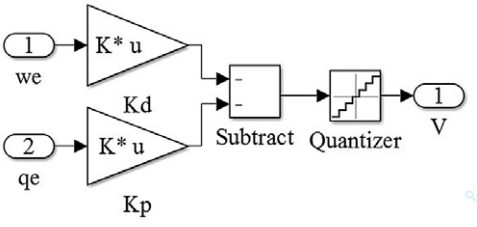


Figure 19. *Simulation model of PD controller.*

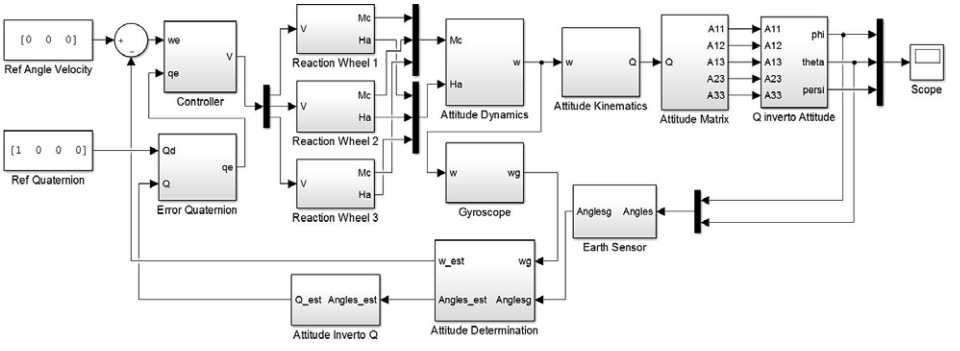


Figure 20. *Simulation platform of the SACS.*

Based on the above analysis, the simulation model of PD controller in the Simulink is showed in Fig. 19. Among them, the input 1 is the error attitude angular velocity ω_e, the input 2 is the error attitude quaternion q_e, and the output 1 is the control voltage V.

Therefore, a complete simulation platform of the SACS is showed in Fig. 20.

https://doi.org/10.1017/aer.2021.79 Published online by Cambridge University Press

Table 1. *Initial simulation parameters [11,14,17]*

Models	Parameters	Values
Controller	K_d	5
	K_p	0.01
Attitude dynamics	J_o	$diag$[0.0109, 0.0506, 0.0509]
Reaction flywheel	J_c	$diag$[0.00191, 0.00191, 0.00191]
	K_m, K_d, K_a	0.053, 0.001, 0.001
	K_n, K_l	0.001, 0.001
Gyroscopes	nd	[0.001, 0.001, 0.001]
	b	[0, 0, 0]
	ng	[0.001, 0.001, 0.001]
	D	$diag$[1/2, 1/3, 1/4]
Earth sensors	b	[0, 0]
	nm	[0.001, 0.001]
Attitude determination	ω_o	0.001rad/s
	K_x, K_y, K_z	0.012, 0.01, 0.008

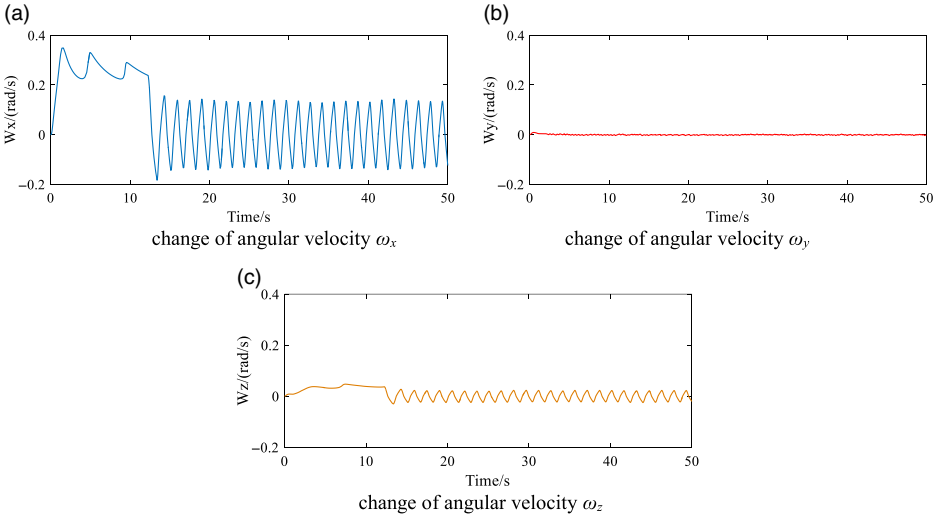


Figure 21. *Change curve of attitude angular velocity.*

3.0 Simulation results analysis

3.1 Results analysis of system simulation platform

In this section, the numerical simulation is executed to verify the performance of the simulation platform of the SACS. The desired angular velocity is ω_d=[0 0 0]^T and the desired quaternion is q_d=[1 0 0 0]^T. The initial parameters of the simulation platform are showed in Table 1.

The change curves of the attitude angular velocity and angle are showed in Figs 21-22. It can be seen that the attitude angular velocity and attitude angle will quickly converge and stabilise in a short time, which indicates that the designed simulation platform has good fastness and stability.

The change curve of control torque of reaction flywheel is showed in Fig. 23. It can be seen that the control torque of reaction flywheel is quickly stabilised within a certain error range, which also verifies the convergence of the designed simulation platform.

The output change curves of the simulation model of the gyroscope and the earth sensor are showed in Figs 24-25. Compared with Figs 21-22, it can be seen that the gyroscope can accurately output

https://doi.org/10.1017/aer.2021.79 Published online by Cambridge University Press

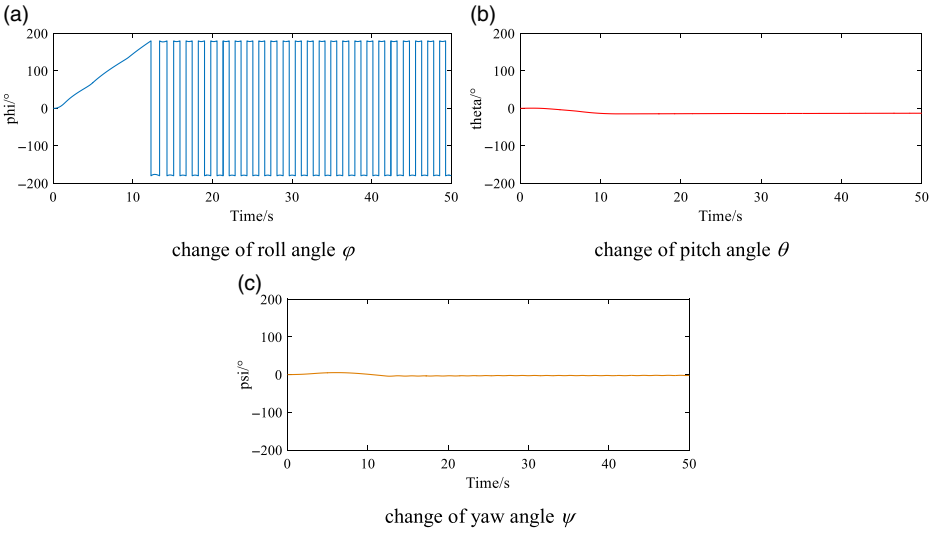


Figure 22. *Change curve of attitude angle.*

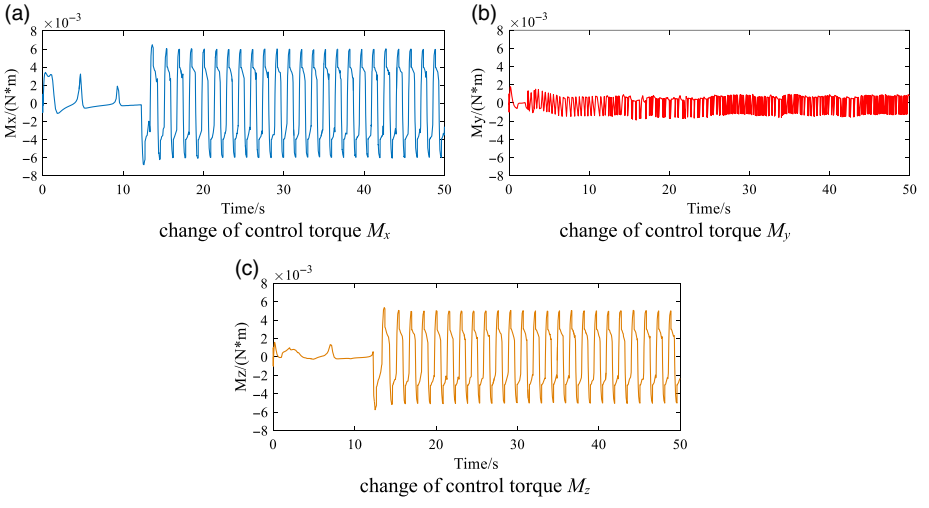


Figure 23. *Change curve of flywheel control torque.*

the angular velocity, and the earth sensor can accurately output the attitude angle, which verifies the correctness and accuracy of the simulation model of attitude sensors.

The changes curve of the attitude angular velocity estimation is showed in Fig. 26. It can be seen that the maximum error range is$\pm$1.5 rad/s, which verifies the correctness and accuracy of the attitude determination model.

In summary, the designed simulation platform of the SACS can output relatively reliable and true control results with good rapidity and stability. At the same time, the output results of the sub-model are also reflect the correctness and accuracy of the simulation platform.

3.2 Simulation and results analysis of component faults

Due to the diversity and complexity of the space environment, the faults occur on the controller, actuator and attitude sensor, which affect the normal operation of the satellite. These faults can be divided into

https://doi.org/10.1017/aer.2021.79 Published online by Cambridge University Press

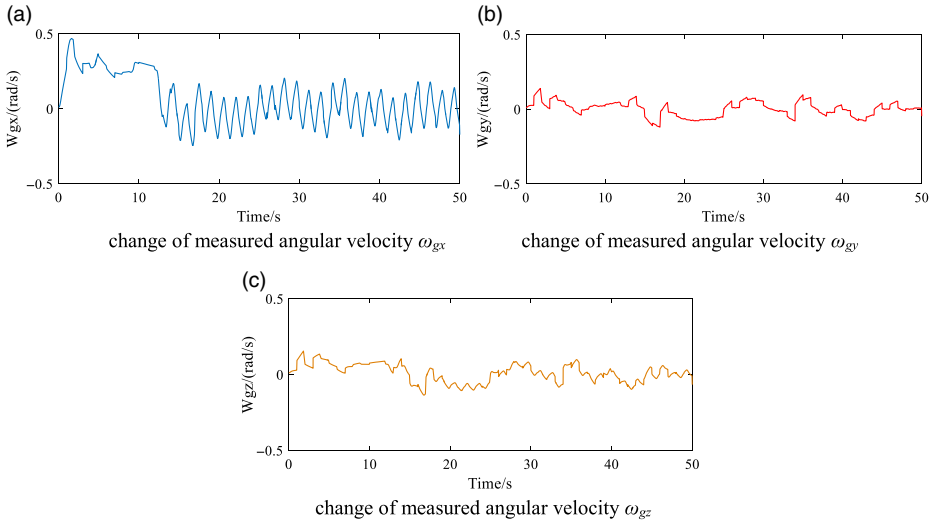


Figure 24. *Change curve of gyro measured output.*

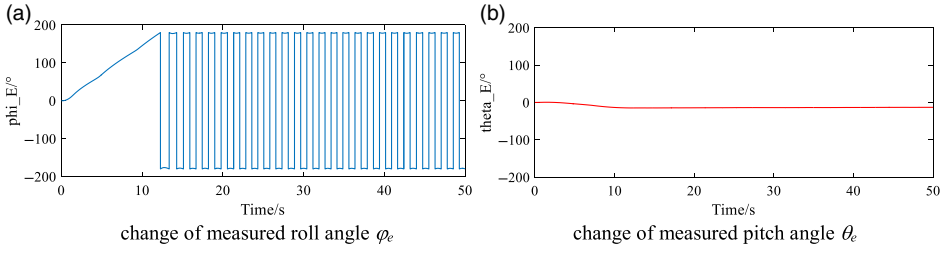


Figure 25. *Change curve of earth sensor measured output.*

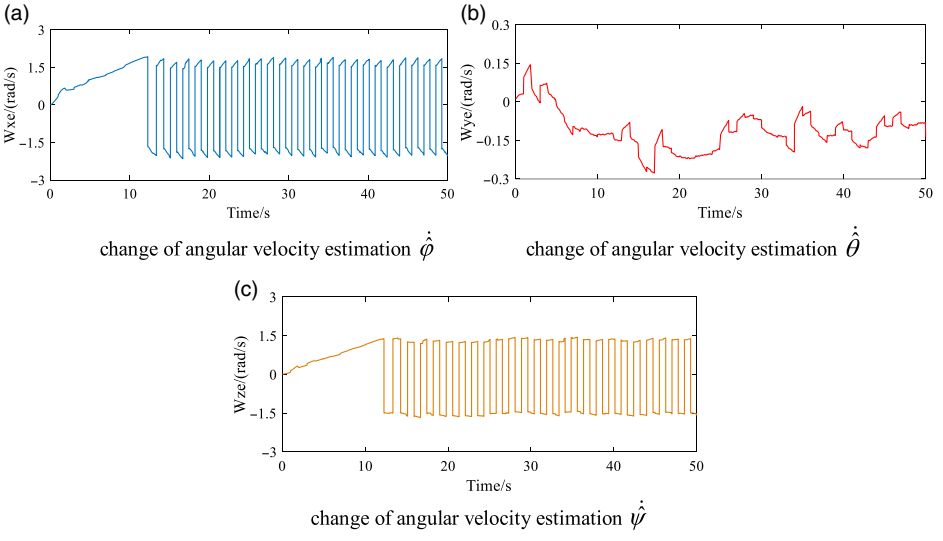


Figure 26. *Change curve of angular velocity estimation.*

https://doi.org/10.1017/aer.2021.79 Published online by Cambridge University Press

three categories based on time characteristics: mutations faults (the faults are often caused by sudden damage to a component), graded faults (the faults are often caused by the long service life of the device and the aging of components) and intermittent faults (the faults are often caused by the poor contact of contact wires and insufficient tolerance) [21]. In order to see the impact of component faults on the performance of the designed simulation platform, we set up controller faults, actuator faults and attitude sensor faults for simulation and analysis in this section.

3.2.1 Simulation analysis of controller faults

Assuming that the intermittent fault appears the controller output between 7 to 8 seconds, the simulation results are showed in Fig. 27. It can be seen that the intermittent faults of the controller will result in a longer response time to reach stability.

If the mutations faults appear the controller output at the 7s, the simulation results are showed in Fig. 28. It can be seen that when the mutation faults appear the controller, the output torque of the reaction flywheel fluctuates greatly, the angular velocity tends to stable after a long time, but there is a large deviation from the expected value, the attitude angle will exhibit a periodic change. The simulation results indicate that the mutations faults of the controller can degrade the performance of the SACS.

3.2.2 Simulation analysis of actuator faults

Since each of the three axes of the satellite is equipped with a reaction flywheel, the faults may occur on the reaction flywheel at different positions. Therefore, the simulation analysis of the impact of the faults of the single reaction flywheel and the combined reaction flywheel on the system performance are done in this section.

3.2.2.1 Fault impact of single reaction flywheel. Assuming that the multiplicative fault appears the reaction flywheel 3, the simulation results of attitude angular velocity and angle are showed in Fig. 29. It can be seen that the angular velocity and attitude angle will eventually change irregularly and not be stable anymore, which indicates that the multiplicative faults of the reaction flywheel damage the stability of the SACS.

If the stuck fault appears the reaction flywheel 3, the simulation results of attitude angular velocity and angle are showed in Fig. 30.

From Fig. 30, it can be seen that when the stuck faults appears on the reaction flywheel, the stability of the SACS is destroyed and the system cannot be stabilized.

3.2.2.2 Fault impact of combined reaction flywheel. The impact of single reaction flywheel fault on system performance has been simulated and analysed. Next, we will analyse the simulation results of the impact of combined reaction flywheel fault on system performance. The specific combination method and simulation results are as follows.

When the fault occur on the reaction flywheel 1 and 2 at the same time, the simulation results of the attitude angular velocity and angle are showed in Fig. 31. It can be seen that the angular velocity on the X axis gradually decreases, and the angular velocity on the Z and Y axes always presents an oscillating form with a large deviation; the attitude angle is always oscillating and is difficult to maintain stable. The simulation results indicate that the stability of the system is undermined.

When the fault occur on the reaction flywheel 1 and 3 at the same time, the simulation results of the attitude angular velocity and angle are showed in Fig. 32. It can be seen that the angular velocity tends to stabilise after a long time; the deviation of the attitude angle will gradually increase. The simulation results indicate that the stability of the system will become worse and worse.

When the fault occur on the reaction flywheel 2 and 3 at the same time, the simulation results of the attitude angular velocity and angle are showed in Fig. 33. It can be seen that the angular velocity on the X axis gradually increases, and the angular velocity on the Y and Z axes always presents an oscillating form with a large deviation; the attitude angle is constantly oscillating and is difficult to maintain stability. The simulation results indicate that the stability of the system has been damaged.

https://doi.org/10.1017/aer.2021.79 Published online by Cambridge University Press

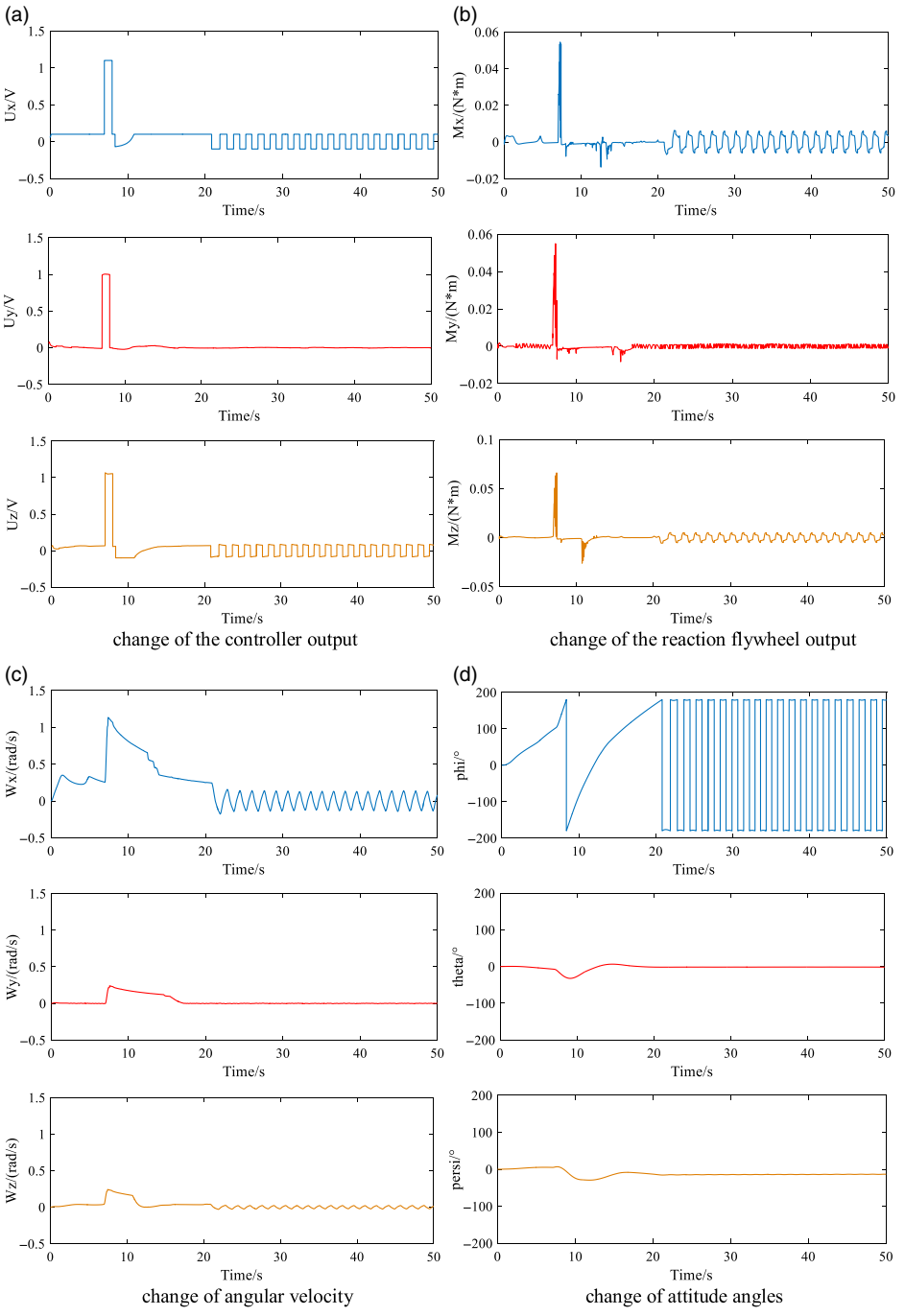


Figure 27. *Simulation results of the controller under intermittent faults.*

When the fault occur on the three reaction flywheels at the same time, the simulation results of the attitude angular velocity and angle are showed in Fig. 34. It can be seen that the angular velocity on the X and Y axes presents a divergent oscillation, and the angular velocity on the Z axis will eventually stabilise, but the deviation very large; the attitude angle has been oscillating and is difficult to maintain stability. The simulation results indicate that the stability of the system has been damaged.

https://doi.org/10.1017/aer.2021.79 Published online by Cambridge University Press

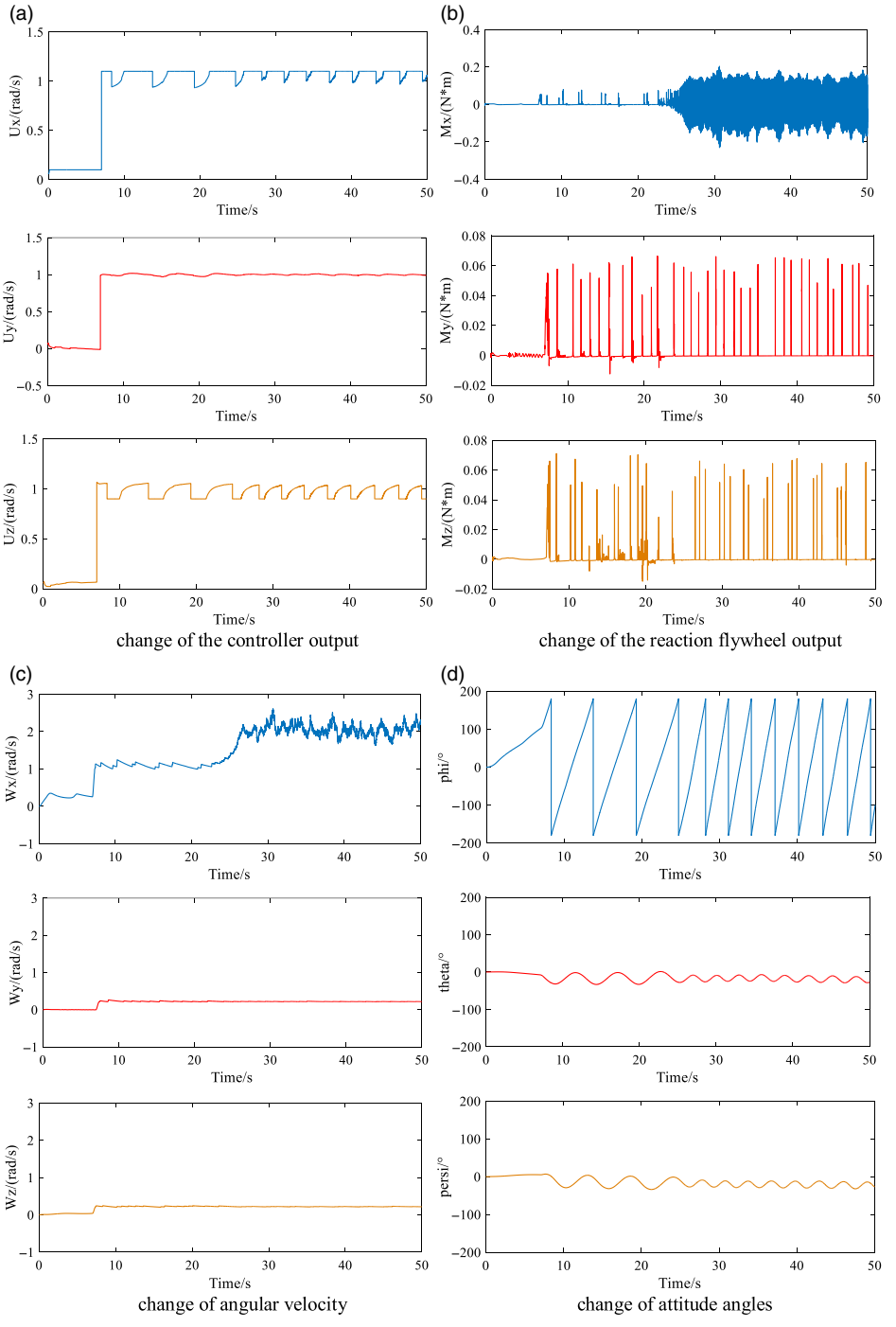


Figure 28. *Simulation results of the controller under mutation faults.*

3.2.3 Simulation analysis of attitude sensors faults

In this paper, the attitude sensor includes gyroscopes and earth sensors. When the gyroscope occurs graded faults and the earth sensor is normal, the simulation results of the attitude angular velocity and angle are showed in Fig. 35. It can be seen that the gradual faults of the gyroscope will cause

https://doi.org/10.1017/aer.2021.79 Published online by Cambridge University Press

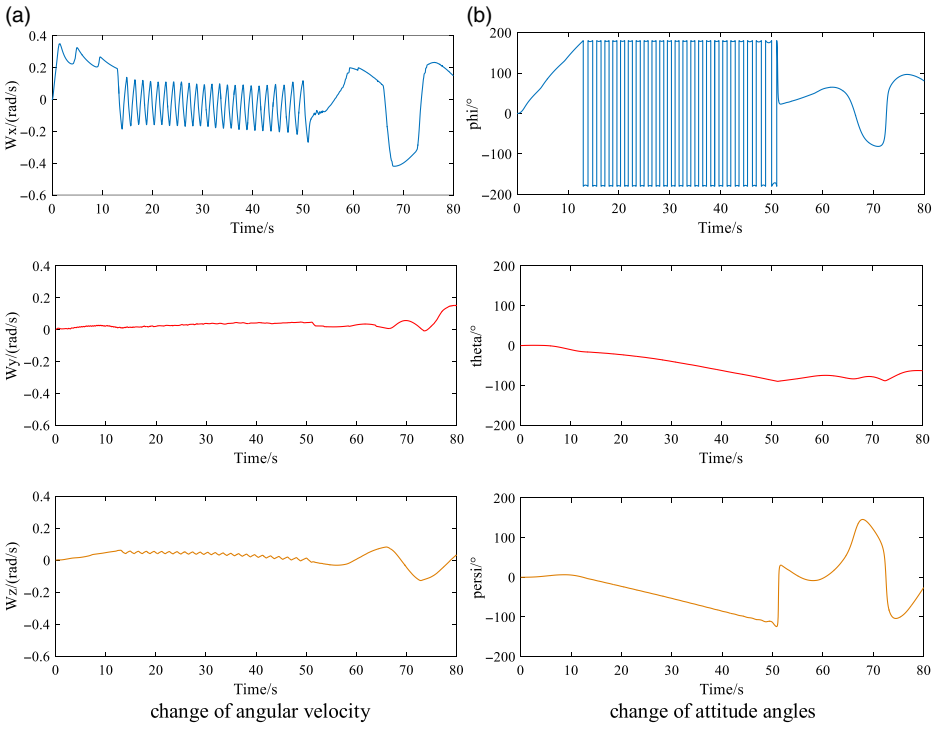


Figure 29. *Simulation results of the reaction flywheel 3 under multiplicative faults.*

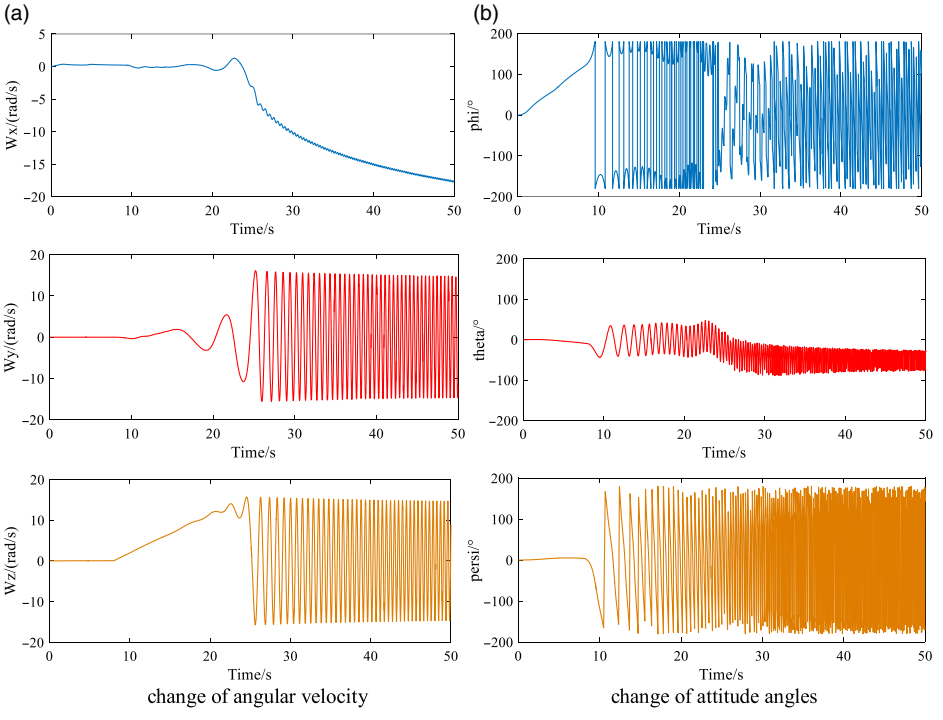


Figure 30. *Simulation results of the reaction flywheel 3 under stuck faults.*

https://doi.org/10.1017/aer.2021.79 Published online by Cambridge University Press

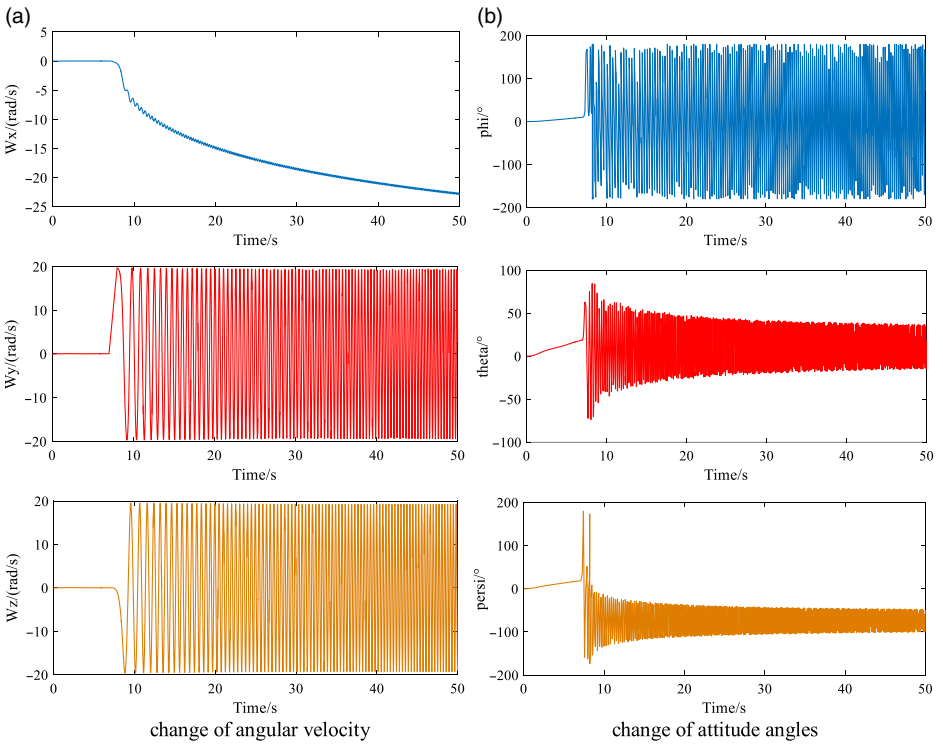


Figure 31. *Simulation results of the reaction flywheel 1 and 2 faults simultaneously.*

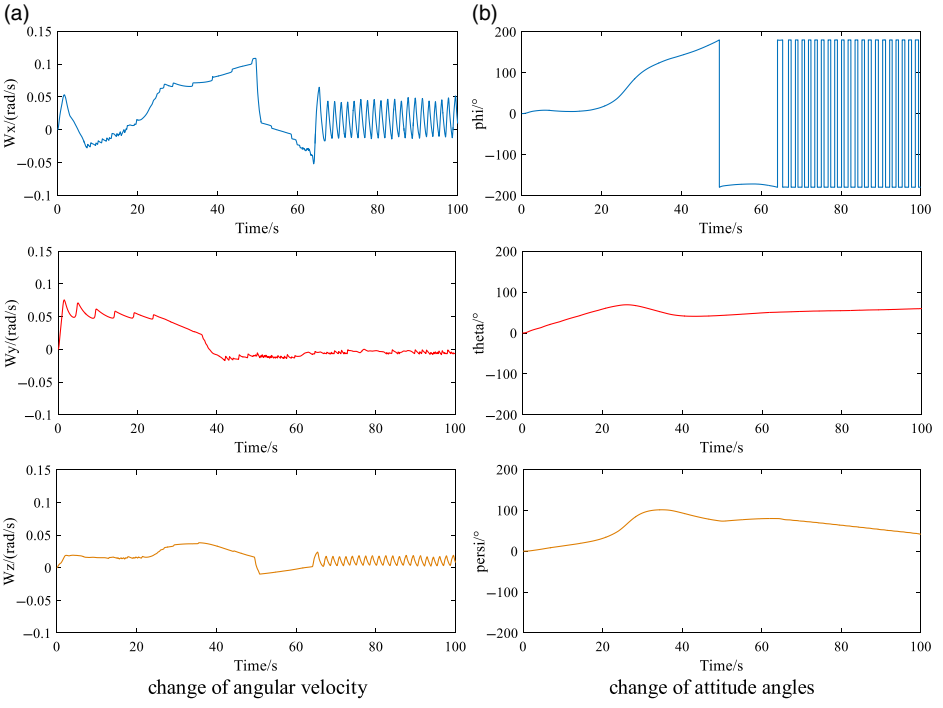


Figure 32. *Simulation results of the reaction flywheel 1 and 3 faults simultaneously.*

https://doi.org/10.1017/aer.2021.79 Published online by Cambridge University Press

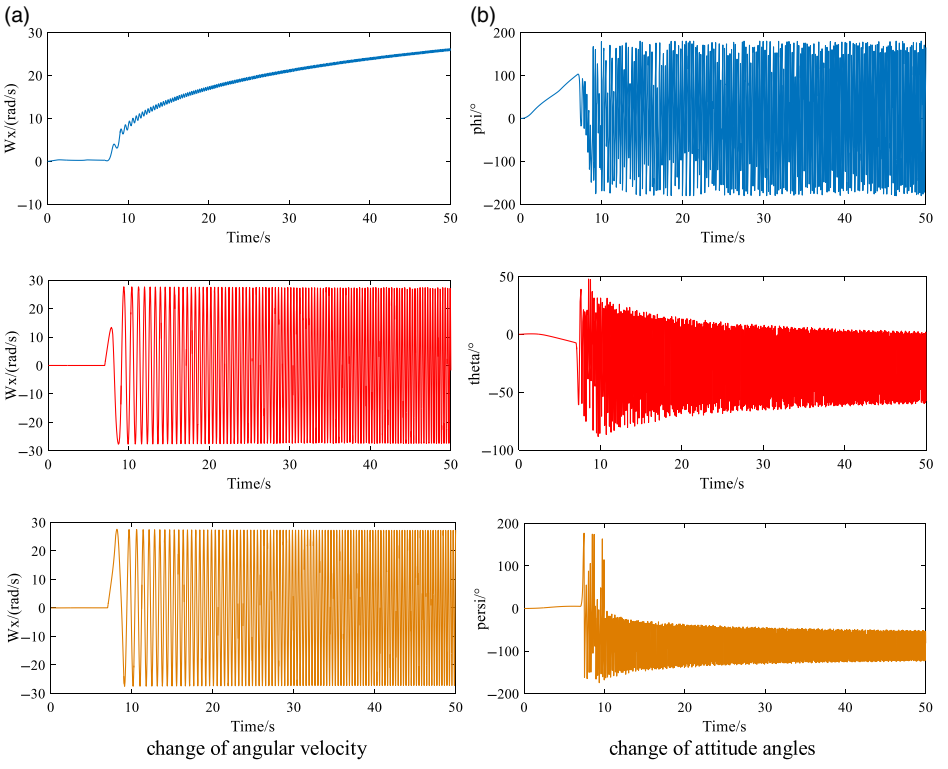


Figure 33. *Simulation results of the reaction flywheel 2 and 3 faults simultaneously.*

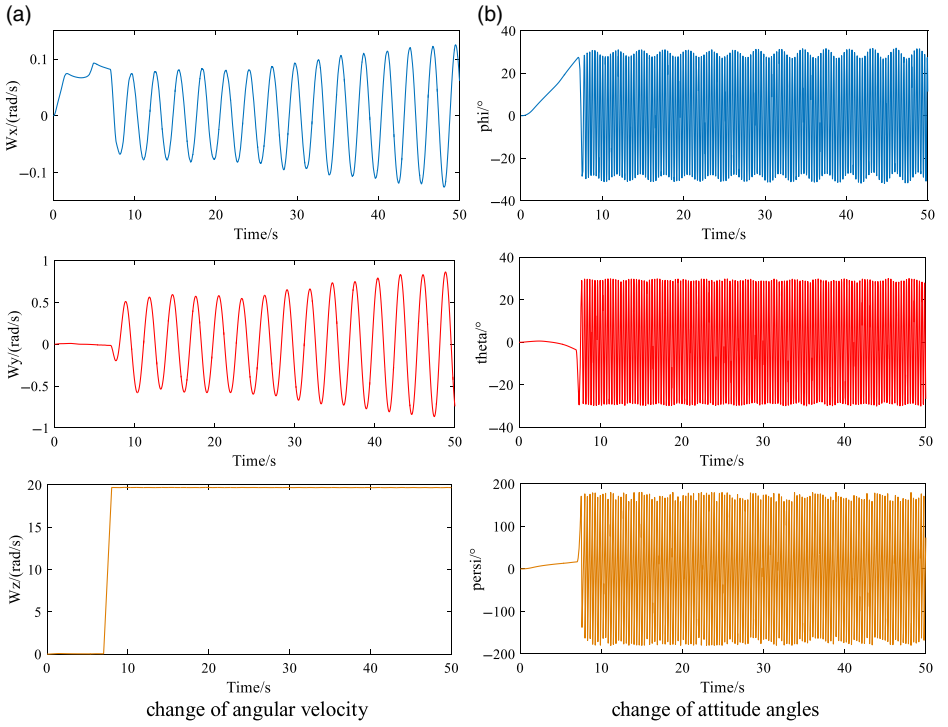


Figure 34. *Simulation results of the three reaction flywheel faults simultaneously.*

https://doi.org/10.1017/aer.2021.79 Published online by Cambridge University Press

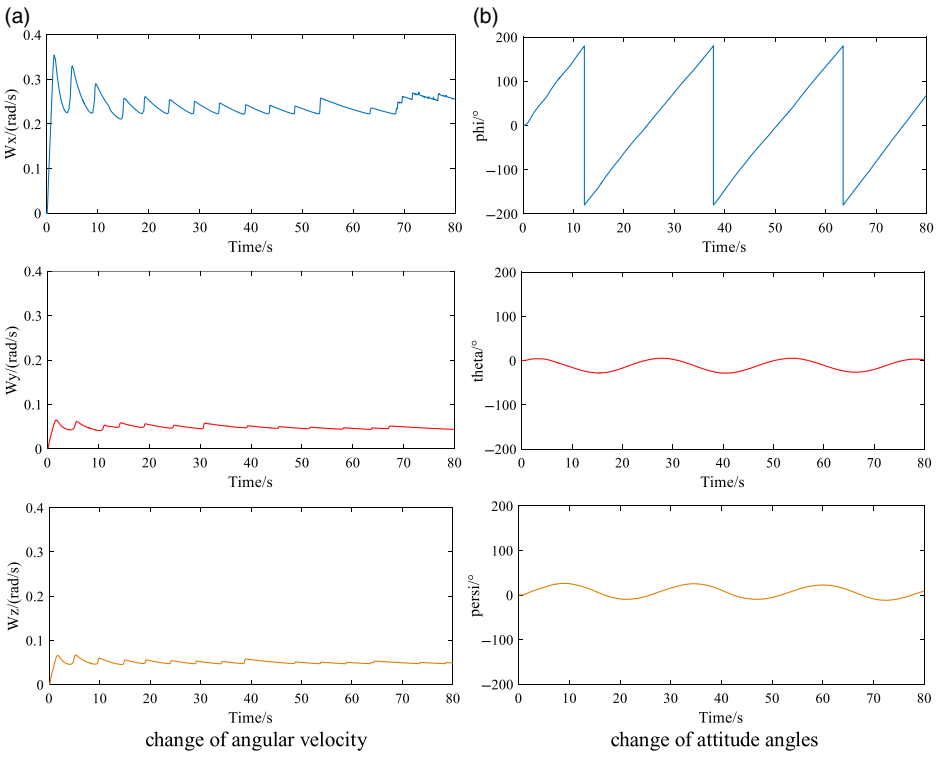


Figure 35. *Simulation results of gyroscope under graded faults.*

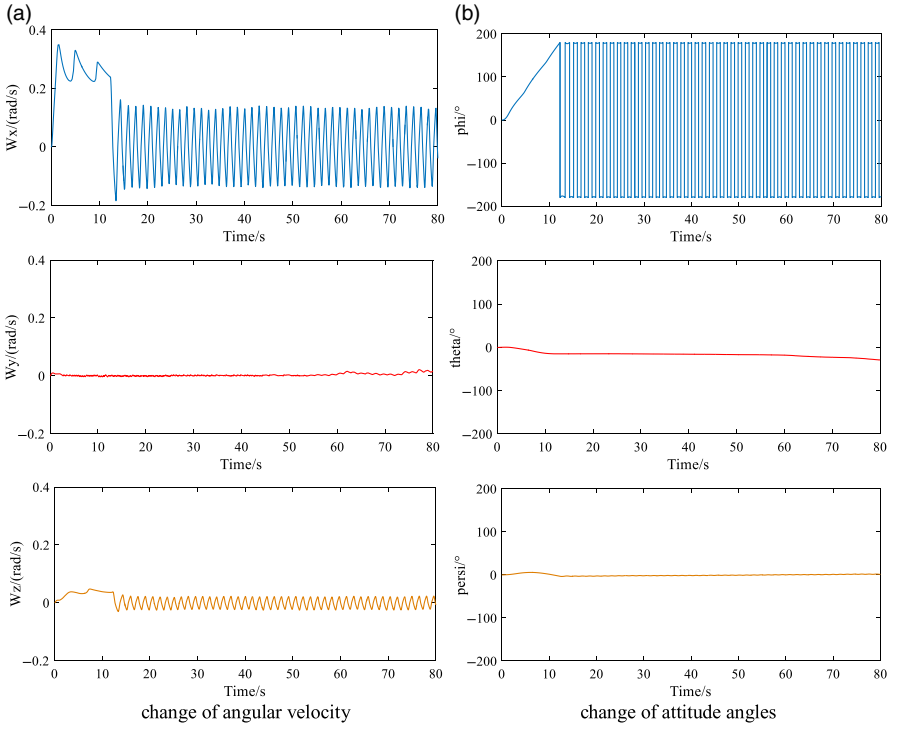


Figure 36. *Simulation results of earth sensor under graded faults.*

https://doi.org/10.1017/aer.2021.79 Published online by Cambridge University Press

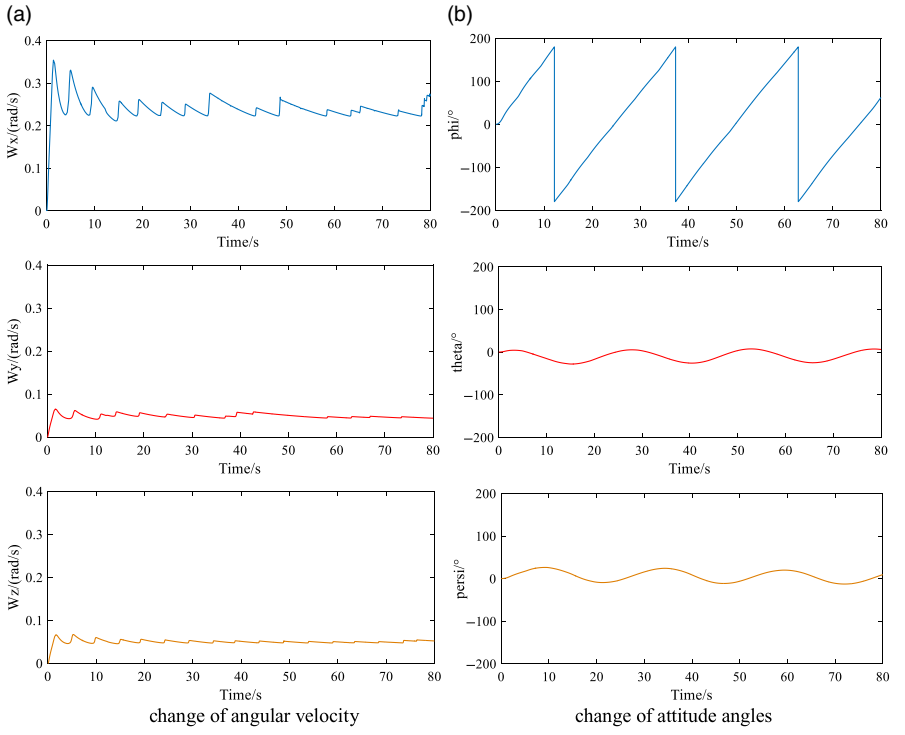


Figure 37. *Simulation results of gyroscope and earth sensor under graded faults.*

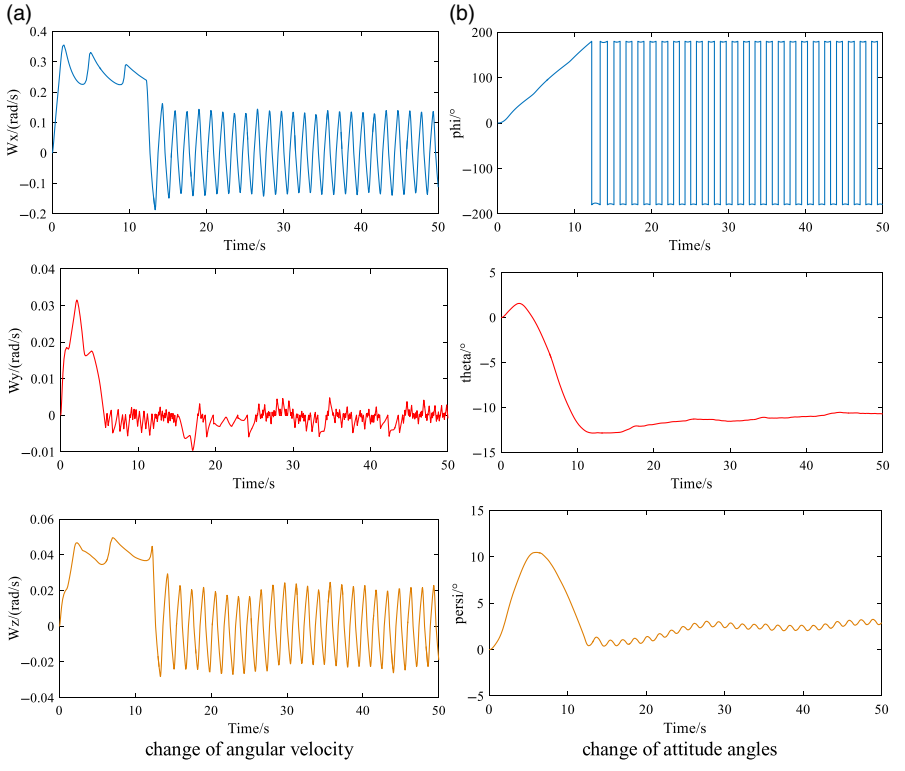


Figure 38. *Simulation results of measurement noise under 10σ.*

https://doi.org/10.1017/aer.2021.79 Published online by Cambridge University Press

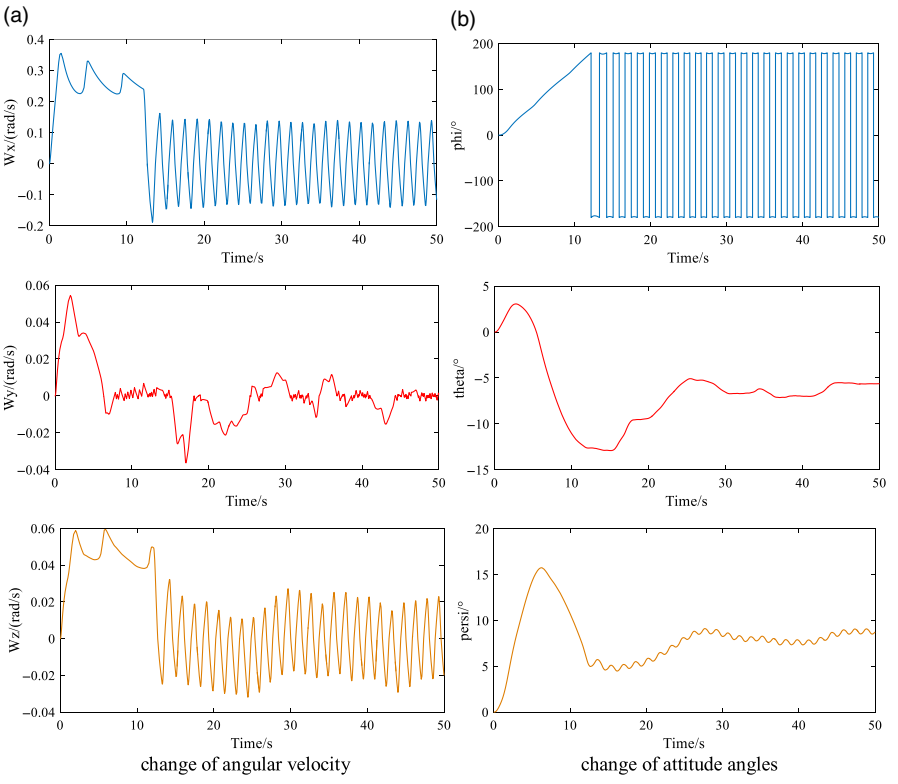


Figure 39. *Simulation results of measurement noise under 50σ.*

the deviation of the angular velocity to increase, and the attitude angle will show a small amplitude periodic oscillation, which will affect the stability of the system.

When the earth sensor occurs the graded faults and the gyroscope is normal, the simulation results of the attitude angular velocity and angle are showed in Fig. 36. It can be seen that the gradual faults of the earth sensor will cause a cumulative deviation in the attitude angle, which will affect the stability of the system.

When the gyroscope and earth sensor occur the graded faults at the same time, the simulation results of the attitude angular velocity and angle are showed in Fig. 37. It can be seen that the gradual faults of the gyroscope and the earth sensor will cause the deviation of the angular velocity to increase, and the attitude angle will show a small amplitude periodic oscillation, which will affect the stability of the system.

3.2.4 Simulation analysis of measurement noise

There is measurement noise in the measurement components. We have carried out the simulation analysis of the influence of measurement noise on attitude angular velocity and angle. The simulation results are showed in the Figs 38-39. It can be seen that measurement noise will affect the attitude angular velocity and angle. The greater the measurement noise, the greater the deviation of the attitude angular velocity and angle.

In summary, the component faults and the measurement noise can affect the performance of the SACS and even destroy the stability of the system, and the simulation result shows that the designed simulation platform can well simulate the impact of system faults on the performance of the SACS.

https://doi.org/10.1017/aer.2021.79 Published online by Cambridge University Press

4.0 Conclusion

In this paper, we build a simulation platform based on Simulink that can simulate the SACS at the component level, which has good speed and stability. Based on the mathematical model, the simulation models of each component are built and integrated into a complete simulation platform. The performance of the simulation platform is verified through numerical simulation.

The simulation results show that the simulation platform can truly reflect the control performance of the SACS at a component level, and can simulate the effect of component faults and measurement noise on the system performance. This simulation platform can provide a good model platform support for verifying the algorithm of fault diagnosis, prediction and tolerant control of the SACS.

This simulation platform is easy to use, improve and expand. In the future work, more specific measurement equipment, such as accelerometers, magnetometers, sun sensors and star sensors, can be added to further improve the control accuracy of the simulation platform.

Acknowledgements. This work is supported by the Natural Science Foundation of China (61973094), the Maoming Natural Science Foundation (2020S004), and the Guangdong Basic and Applied Basic Research Fund Project (2020B1515310003).

References

1. Han, Y., James, D.B. and Cui, N.G. Adaptive Fault-Tolerant Control of Spacecraft Attitude Dynamics with Actuator Failures, *J. Guid. Control. Dyn.*, 2015, **38**, (10), pp 2033–2042. https://doi.org/10.2514/1.G000921
2. Cui, R.J. Design and Research of the Integrated Simulation Platform for Satellites Attitude Control System, Zhejiang University, Thesis, 2017 https://kns.cnki.net/KCMS/detail/detail.aspx?dbname=CMFD201701&file-name=1017051028.nh.
3. Yu, Y.T. and Liang, J.H. Attitude Determination and Control of Small Satellites Based on Simulink, *Comput. Simul.*, 2006, (11), pp 71–74. doi: CNKI:SUN:JSJZ.0.2006-11-018
4. Bai, X.L. and Bei, C. Rapid Design of Small Satellite Attitude Control System Based on Simulink, *the 5th Chinese and Overseas Aerospace Science and Technology Seminar*, 2009. http://www.doc88.com/p-3458094045058.html
5. Peng, R. and Bai, J.X. Research on Universal Hardware-in-Loop Simulation Test System of Satellite AOCS, *Digit. Technol. Appl.*, 2011, (09), pp 58–59+61. doi: 10.19695/j.cnki.cn12-1369.2011.09.040
6. Tortora, P., Giulietti, F., Corbelli, A., et al. ALMASat attitude control hardware-in-the-loop simulation, *AIAA 57th International Astronautical Congress*, 2006, **7**, pp 4787–4795. https://doi.org/10.2514/6.IAC-06-C1.P.2.03
7. Qiao, L., Zhang, M., Osborne, B., et al. Attitude Determination and Control System (ADCS) of UNSW QB50 project "UNSW EC0", *Proceedings of the 13th Australian Space Science Conference, Sydney, Australia*, 2013. Google Scholar.
8. He, S.J., Yang, L. and Chen X.Q. Design of a Satellite Orbit Prediction Visualization Platform Based on LabVIEW and STK, *Sci. Technol. Eng.*, 2011, **11**, (23), pp 5702–5706+5717. doi: CNKI: SUN: KXJ S.0.2011-23-053
9. Haddox, P.G. The development of a hardware-in-the-loop attitude determination and control simulator for IlliniSat-2, *52nd Aerospace Sciences Meeting*, 2014, 0007. Google Scholar.
10. Ure, N.K., Kaya, Y.B., Inalhan, G. The Development of a Software and Hardware-in-the-Loop Test System for ITU-PSAT II nano satellite ADCS, *2011 Aerospace Conference*, 2011, pp 1–15. Google Scholar.
11. Liang, X.J. Simulation of 3-Axis Stable Satellite Attitude Control System Based on Modularization, *Comput. Simul.*, 2012, **29**, (09), pp 91–95. doi: CNKI:SUN:JSJZ.0.2012-09-023
12. Tu, S.C. *Satellite Attitude Dynamics and Control*, Beijing: China Astronautic Publishing House, 2009. https://xueshu.baidu.com/usercenter/paper/show?paperid=78be72110e9159dfe35b34a6f4487da6
13. Chen, F.F., Zhang, G.F. and Chen, Y.F. Non-linear modelling and simulation technique for momentum wheel of small satellites, *J. Astronaut.*, 2003, (06), pp 651–655. doi: CNKI:SUN:YHXB.0.2003-06-022
14. Jiang, R., Wei, J.L. and Cen, Z.H. Simulation Modelling of Satellite Attitude Control System Based on Quaternion Feedback, *J. Syst. Simul.*, 2009, **21**, (19), pp 6260–6265. doi: CNKI:SUN:XTFZ.0.2009-19-070
15. Bauer, R.J., Hong, T. and Hughes, P.C. Augmented system identification of reaction wheel friction. *Canad. Aeronau. Spac. J.*, 2001, **47**, (2), pp 51–56. Google Scholar.
16. Zhang, R.W. *Satellite Orbit Attitude Dynamics and Control*, Beihang University Press, 1998, Beijing. Google Scholar.
17. Bian, Z.Q., Cheng, W.Q. and Xue, X.B. Satellite Attitude Determination Algorithm Based on Gyro and Star-sensor, *Spacecr. Eng.*, 2011, **20**, (02), pp 29–34. doi: CNKI:SUN:HTGC.0.2011-02-007
18. Zhu, Q.H. and Li, Y.B. Extended Kalman Filter for Attitude Determination Using Gyros and Quaternion, *Aerosp. Shanghai*, 2005, (04), pp 1–5+59. doi: 10.19328/j.cnki.1006-1630.2005.04.001
19. Yang, B., Yu, X.Y. and Miao, J. A Method of Starlight Navigation Using the Infrared Horizon Sensor, *J. Astronaut.*, 2016, **37**, (09), pp 1089–1097. doi: 10.3873/j.issn.1000-1328.2016.09.008
20. Wang, H.J., Xing, F. and You, Z. Numerical analysis and experiment study of navigation algorithm withtriple-FOV infrared earth sensor, *Chin. J. Sci. Instrum.*, 2016, **37**, (06), pp 1201–1209. doi: 10.19650/j.cnki.cjsi.2016.06.001

https://doi.org/10.1017/aer.2021.79 Published online by Cambridge University Press

21. Han, Y. Spacecraft Attitude Fault-Tolerant Control Methods with Actuator Fault, Harbin Institute of Technology, Thesis, 2016. https://kns.cnki.net/KCMS/detail/detail.aspx?dbname=CDFDLAST2017&filename =1016739814.nh
22. Schwabacher, M. Machine learning for rocket propulsion health monitoring, *SAE Trans.*, 2005, pp 1192–1197. https://www.jstor.org/stable/44682813

Cite this article: Song H., Hu S.L., and Chen W.Z. (2022). Simulink-based simulation platform design and faults impact analysis of attitude control systems. *The Aeronautical Journal*, **126**, 475–499. https://doi.org/10.1017/aer.2021.79
https://doi.org/10.1017/aer.2021.79 Published online by Cambridge University Press